Journal of Power Sources 256 (2014) 244–249

Contents lists available at ScienceDirect

Journal of Power Sources

journal homepage: www.elsevier.com/locate/jpowsour

Rapid charge and discharge property of high capacity lithium ion battery applying three-dimensionally patterned electrode

Akira Izumi [a], Masakazu Sanada [a], Koji Furuichi [a], Kuniko Teraki [a], Takeshi Matsuda [a], Kenta Hiramatsu [a], Hirokazu Munakata [b], Kiyoshi Kanamura [b,*]

[a] Dainippon SCREEN Mfg. Co., Ltd, 322 Furukawa-cho, Hazukashi, Fushimi-ku, Kyoto 612-8486, Japan
[b] Graduate School of Urban Environmental Sciences, Tokyo Metropolitan University, 1-1 Minami-Osawa, Hachioji, Tokyo 192-0397, Japan

HIGHLIGHTS

- 3D-patterned electrodes with various types of line patterns were fabricated.
- The effect of pattern specifications on the electrode performance was evaluated.
- The better rate capability is obtained for the narrower width of electrode line.
- The line height and line space hardly affect the rate capability of electrode.
- The charge-transfer resistances hardly depend on the electrode pattern.

ARTICLE INFO

Article history:
Received 15 September 2013
Received in revised form
8 January 2014
Accepted 14 January 2014
Available online 24 January 2014

Keywords:
Lithium-ion battery
Lithium titanium oxide
Three-dimensionally patterned electrode
Rate capability

ABSTRACT

The cells applied with a three-dimensionally (3D) patterned $Li_4Ti_5O_{12}$ (LTO) electrode showed good performance as a rechargeable lithium-ion battery. The 3D-patterned electrode was fabricated with a printing apparatus and has many lined patterns with a high aspect ratio standing in line on a current collector. The cell using 3D-patterned electrode showed much better rate capability than that using a conventional flat electrode. In this research, cyclic voltammetry was carried out to investigate the mechanism realizing the high rates of charging and discharging in 3D-patterned electrode. Various types of line patterns were fabricated for 3D electrode by using LTO electrode slurry, and the influences of basic specifications of electrode structure (the space between two neighboring electrode lines, the height and width of electrode) on the charge and discharge characteristics were evaluated to optimize the electrode pattern. In addition, the electrode performance was discussed from the viewpoints of ohmic resistance and charge-transfer resistance of the cells with 3D-patterned and conventional flat electrodes.

1. Introduction

Lithium-ion battery has higher energy density than other conventional rechargeable batteries, namely the amount of energy that can be stored per unit volume and weight is large [1]. Hence recently, the lithium-ion battery is started to be used for electric vehicles [2]. However, its performance is not still enough in both energy and power densities. Therefore, research and development aiming at higher energy density and higher rate performance of lithium-ion batteries are conducted intensively [3,4]. The rate performance of lithium-ion battery depends on the diffusion rate of lithium-ion, particularly in porous composite anode and cathode. High performance requires high current of electrochemical reactions. In order to promote diffusion of the lithium-ion in the cell, it is focused on to increase the surface area of active material layer and to decrease the diffusion length of lithium-ion between anode and cathode [5–9]. On the other hand, higher energy density requires the higher mass per unit volume of active material in the electrode. However, the diffusion resistance of lithium-ions in the electrode increases with increasing the electrode density. Consequently, it is difficult to achieve both high energy density and high rate performance simultaneously in conventional lithium-ion batteries [10].

We have been focusing on three-dimensionally (3D) integrated electrode structure as one of the effective solutions to realize the high rate performance without sacrificing the energy density of batteries [11–14]. In our previous report, a printing method combined with the manufacturing process of electrode was developed

* Corresponding author. Tel./fax: +81 42 677 2828.
E-mail address: kanamura@tmu.ac.jp (K. Kanamura).

0378-7753/$ – see front matter © 2014 Elsevier B.V. All rights reserved.
http://dx.doi.org/10.1016/j.jpowsour.2014.01.067

aiming at a large scale production of 3D structured electrodes for the upcoming demands in battery development [11]. The cyclic voltammogram of the half cell with 3D $Li_4Ti_5O_{12}$ cathode and lithium metal anode indicated a couple of reversible peaks assignable to the lithiation and delithiation of lithium-ions to $Li_4Ti_5O_{12}$ and from $Li_7Ti_5O_{12}$, suggesting that the 3D-patterned electrode fabricated by the printing apparatus works effectively. Furthermore, it was confirmed that the capacity retention at 5 C for the 3D-patterned electrode was 2.3 times larger than that obtained for a conventional flat electrode. These results strongly support the enhancement of lithium-ion diffusion by 3D patterning of electrode.

In this study, cyclic voltammetry was carried out to investigate the mechanism realizing the high rates of charging and discharging in 3D-patterned electrodes. The interfacial resistance difference between the cells with 3D-patterned and conventional flat electrodes was also analyzed in AC impedance measurement. In addition, the influences of basic specifications of electrode (the space between two neighboring electrode lines, the height and width of electrode) on the charge–discharge characteristics were thoroughly evaluated.

2. Experimental

2.1. Fabrication of 3D-patterned and conventional flat electrodes

Cathode consisted of 80 wt% $Li_4Ti_5O_{12}$ (LTO, ISHIHARA SANGYO KAISHA, LTD.), 10 wt% acetylene black (AB, DENKI KAGAKU KOGYO KABUSHIKI KAISHA, average diameter: 35 nm) and 10 wt% poly(vinylidene difluoride) (PVdF, KISHIDA CHEMICAL Co., Ltd.) binder. Their mixture was dispersed into *N*-methylpyrrolidinone (NMP) to make the composite slurry. The weight ratio of NMP in the slurry was about 50 wt% for 3D-patterned electrodes. The slurry condition of high viscosity was selected for fabricating 3D-patterned electrodes by using the printing system described in our former report [11]. By using these materials, the 3D-patterned electrodes with 1 mA h cm^{-2} were prepared. For comparison, a conventional flat electrode was also fabricated. The composite slurry for the flat electrode consisted of LTO, AB and PVdF in the weight ratio of LTO:AB:PVdF = 8:1:1 same as that for the 3D electrode. This mixture was dispersed in NMP. The weight ratio of NMP in the slurry was controlled to be approximately 65%. The composite slurry was applied onto an aluminum current collector by using a commercial applicator (YASUDA SEIKI SEISAKUSHO, LTD.). The gap between applicator and the current collector was adjusted to control the electrode capacity per unit area for 1 mA h cm^{-2} which is as same as the 3D-patterned electrode. After the application, both types of electrodes were dried at 80 °C for 5 h under vacuum condition. Only the flat electrodes were then pressed at 30 MPa for 2 min before use. On the contrary, 3D-patterned electrodes were not pressed to maintain their structures. The shape of electrodes was observed with a laser microscope (VK-9500, Keyence).

2.2. Fabrication of cells

2032 coin-type cells were fabricated for the 3D-patterned and conventional flat electrodes by using lithium metal anode. A conventional porous polypropylene film was used as a separator. The electrolyte was 1 mol dm^{-3} $LiPF_6$ in an organic liquid mixture consisting of ethylene carbonate (EC) and ethyl methyl carbonate (EMC) (1:1 volume). Current collector was an aluminum foil. The cells were assembled in a glove box under argon atmosphere.

2.3. Evaluation of electrochemical performance

Hereafter, all the electrode potentials were referred to Li/Li^+. Cyclic voltammetry has been carried out respectively at a potential sweep rate of 20, 50 and 100 mV min^{-1} at 25 °C by using a potentiostat (HZ-3000, Hokuto Denko). Charge–discharge behaviors of the cells were recorded with a charge–discharge controller under constant current density (HJ-1001SD8, Hokuto Denko). The charge–discharge voltage region was from 1.0 V to 3.0 V and current density was 0.2 C. AC impedance measurement was performed at every 20% state of charge (SOC) at 25 °C using a potentiostat (SI1287, Solartron) and a frequency response analyzer (1252A, Solartron). The cell was discharged at the rate of 0.2 C from SOC 100% to 0%. The frequency range was 1 MHz–1 Hz, and the amplitude of voltage was 5 mV.

3. Results and discussion

3.1. Electrode structure

Fig. 1(a) shows the specifications of electrode design, in which the height (*H*) and width (*W*) of electrode line, and the space between two neighboring electrode lines are 150 μm, 70 μm and 80 μm, respectively. From the laser microscope image shown in Fig. 1(b), it was confirmed that the 3D-patterned LTO electrode fabricated using a printing apparatus had a well-defined structure according to the electrode design although the head of electrode line became slightly round. The aspect ratio (*H* value/*W* value) of this electrode pattern is about 2, but which can be increased up to over 4 (for example $W = 70$ μm and $H = 300$ μm) by using the printing apparatus manufactured by us. The size of applied area on an aluminum foil was 30 mm × 50 mm, in which no significant defect such as a shortage of the electrode line was observed.

3.2. Cyclic voltammograms

Cyclic voltammetry was carried out at 20, 50 and 100 mV s^{-1} for conventional flat and 3D-patterned electrodes, respectively.

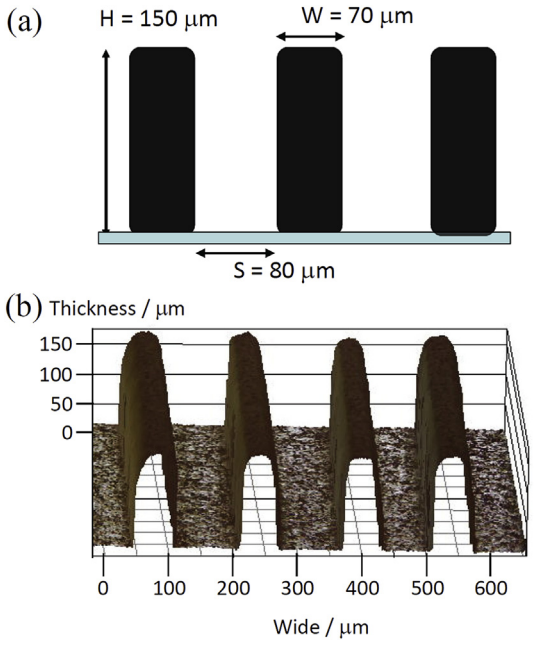

Fig. 1. The specifications of electrode design (a) and a typical laser microscope image of the prepared electrode (b).

Fig. 2 shows the cyclic voltammograms (CVs) of the cells applied with the conventional flat (a) and 3D-patterned LTO (b) electrodes. All the CVs were collected at the third cycle. Both charge and discharge peaks observed for the 3D-patterned electrode were sharper than those for the flat one. The charge current in the anodic sweep became nearly 0 A g^{-1} after 2.0 V for 20 mV min^{-1} and after 2.4 V for 50 mV min^{-1}, respectively. On the other hand, the charge current for the flat electrode still flew a little in the same conditions. This result shows 3D-patterned electrode has a lower over-potential for charge and discharge reactions than those of flat one. Table 1 shows the cell capacity estimated by integration of CV current peaks in Fig. 2. It was confirmed that both types of electrodes can be fully charged at 20 mV min^{-1}, which is a relatively slow scan rate condition. The 3D-patterned electrode had almost the same capacity when increasing the scan rate from 20 to 50 mV min^{-1}. However, the flat electrode could not be fully charged at the 50 mV min^{-1} condition. From these results, it can be found that lithium-ion diffusion rate in the cell with 3D-patterned electrode is faster than that with flat electrode, and rapid charge and discharge can be realized using the 3D-patterned electrode.

Table 1
Cell capacity estimated by integration of CV current peaks in Fig. 2.

Electrode type		Cell capacity/mA h g^{-1}		
		20 mV min^{-1}	50 mV min^{-1}	100 mV min^{-1}
3D-patterned electrode	Charge	158.0	154.9	121.8
	Discharge	157.8	154.8	113.0
Conventional flat electrode	Charge	154.9	127.9	116.7
	Discharge	154.8	110.7	93.0

3.3. AC impedance measurements

Fig. 3 shows the galvanostatic charge and discharge curves at 0.2 C rate for the cells with the conventional flat (a) and 3D-patterned LTO (b) electrodes. Charge and discharge were stopped at every 20% SOC, and the electrochemical AC impedance measurement was performed. The ohmic resistance (R_s) and charge-transfer resistance (R_{ct}) were calculated by using the Nyquist plots obtained from the impedance measurements. R_s was assigned to an intercept of the semicircle at Z' abscissa in a low frequency region, and R_{ct} was calculated from the diameter of semicircle. The details of this calculation method are shown in Fig. 4, and the calculated R_{ct} values are shown in Fig. 5. The R_s values for the 3D-patterned electrode were relatively small, and the average R_s values for the 3D-patterned and flat electrodes were 6.98 Ω and 7.78 Ω, respectively. R_{ct} value during charging was a little smaller than that of discharging regardless of the electrode type. However, it was found that R_{ct} values of 3D-patterned electrode were smaller than those of the flat one at SOC 0 and 20%. The reason for this difference is unclear, but there is only a slight difference of resistance between the both types of electrodes. Therefore, it can be considered that

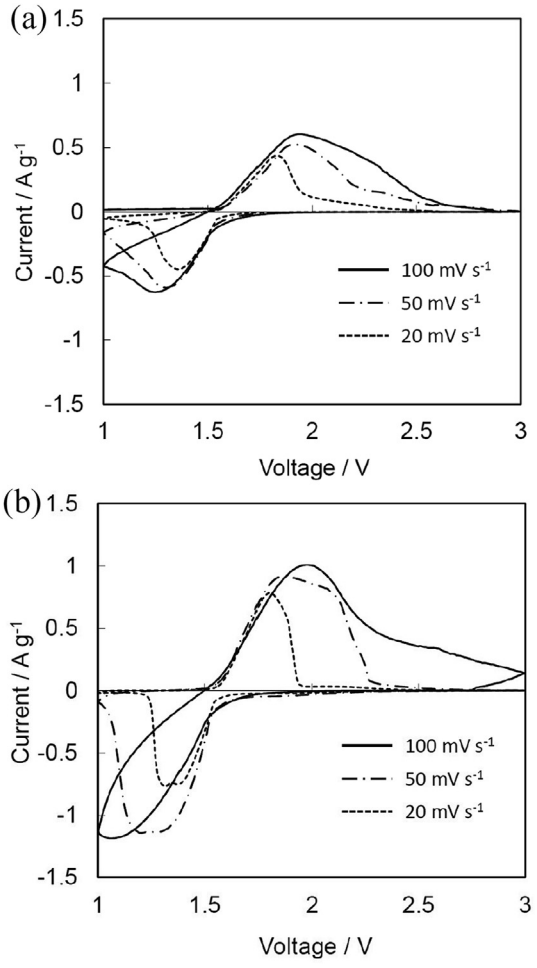

Fig. 2. Cyclic voltammograms of the cells with the conventional flat (a) and 3D-patterned LTO (b) electrodes at 20, 50 and 100 mV min^{-1}.

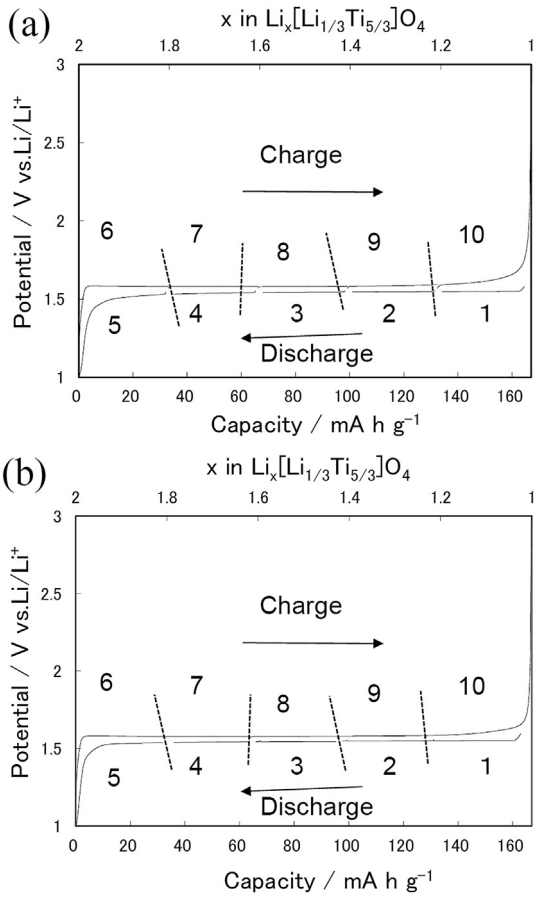

Fig. 3. Galvanostatic charge and discharge curves at 0.2 C rate for the cells with the conventional flat (a) and 3D-patterned LTO (b) electrodes.

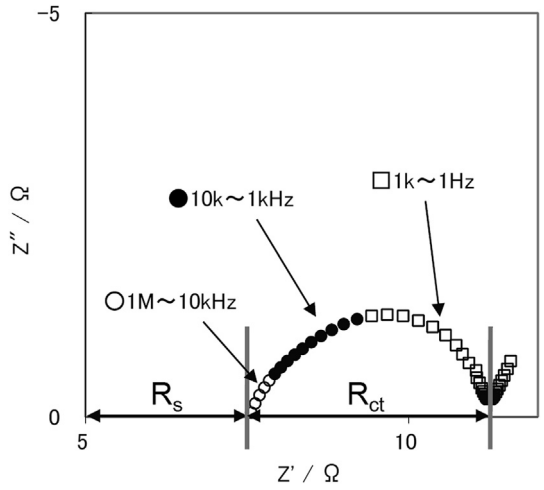

Fig. 4. Schematic showing R_s and R_{ct} in Nyquist plot with three different frequency regions of 1 MHz–10 kHz (○), 10 kHz–1 kHz (●) and 1 kHz–1 Hz (□).

almost equal resistance values were obtained since the same active materials were used for both cases.

3.4. Influence of the specifications of 3D-patterned electrode on battery properties

Basic specifications of 3D-patterned electrode on the charge and discharge characteristics were evaluated. The basic structure of 3D-patterned electrode is the same shown in Fig. 1. The space (S) between two neighboring LTO electrode lines was selected as 100, 50, 25 and 15 μm. The width (W) and height (H) of the LTO electrode line were fixed to 100 and 65 μm, respectively. The charge and discharge test were carried out at constant currents ranging from 0.1 C to 10 C. Fig. 6 shows the capacity retentions at various C rates for the cells with 3D-patterned LTO cathode/lithium anode. The space (S) between two neighboring LTO electrode lines does not affect the capacity retention level except the cases of S = 15 and 25 μm at 5 and 10 C. Fig. 7 shows the capacity per unit area on C rate for the cells with 3D-patterned LTO cathode/lithium anode as a function of the space (S) between two neighboring LTO electrode

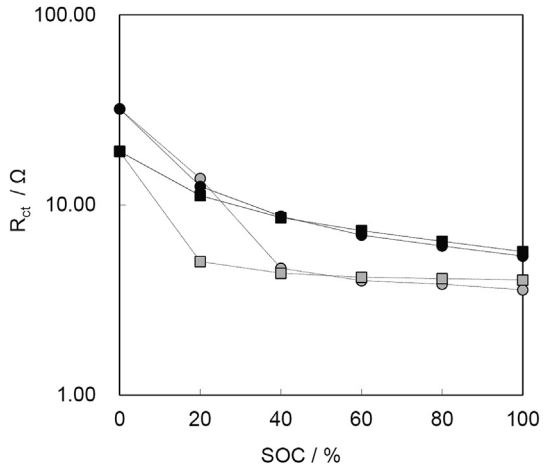

Fig. 5. R_{ct} as a function of SOC, calculated for the cells with the conventional flat (circle symbols) and 3D-patterned LTO (square symbols) during the charge (black symbols) and discharge (gray symbols) processes shown in Fig. 3. R_{ct} values were collected according the number shown in Fig. 3.

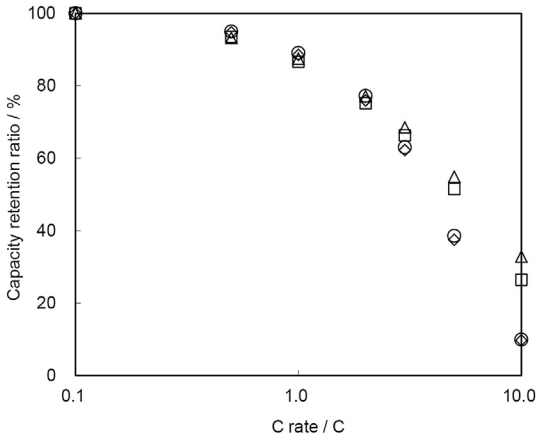

Fig. 6. Dependency of capacity retention ratios on the space (S) between two neighboring LTO electrode lines at various C rates, estimated using the cells with 3D-patterned electrodes of S = 100 μm (△), 50 μm (□), 25 μm (○), 15 μm (◇). The width (W) and height (H) of the electrode line were fixed to 100 and 65 μm, respectively.

lines. This data suggests that capacity can be increased by reducing space.

The influence of the 3D-patterned electrode height (H) was also evaluated. The height of LTO electrode line was selected as 50, 70 and 90 μm. On the other hand, the space between two neighboring LTO electrode lines and the width of the LTO electrode line was fixed to 100 μm (S, W = 100 μm), respectively. The charge and discharge test was carried out in the same conditions for Fig. 6. Fig. 8 shows the capacity retentions at various C rates for the cells with 3D-patterned LTO cathode/lithium anode. Fig. 9 shows the capacity per unit area on C rate for the same cells. These results show that the increase in the electrode height (H) does not affect the capacity retentions at every C rate, but the capacity per unit area can be improved. For further investigation on the height of 3D-patterned electrode, internal resistance at the time of charge (R_c) and discharge (R_d) were estimated by AC impedance method for the 3D-patterned electrodes with H = 50, 70 and 90 μm. As showed in Fig. 10, all the 3D-patterned electrodes showed about 15 and 30 Ω g^{-1} as R_c and R_d, respectively. This result clearly suggests that both R_c and R_d are hardly affected by the height of 3D electrode.

The influence of the 3D electrode width (W) was also evaluated, in which the LTO electrode lines with W = 70 and 100 μm were compared. The height (H) was controlled as the electrode capacity (cross section) became approximately equal. Consequently, H was

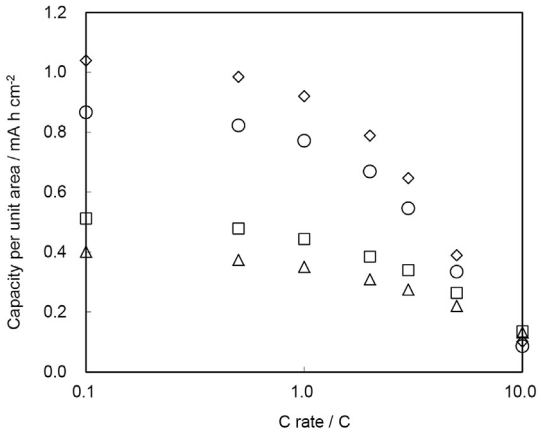

Fig. 7. Capacity dependency on C rate for the cells with 3D-patterned electrodes of different S values (Fig. 6): S = 100 μm (△), 50 μm (□), 25 μm (○), 15 μm (◇).

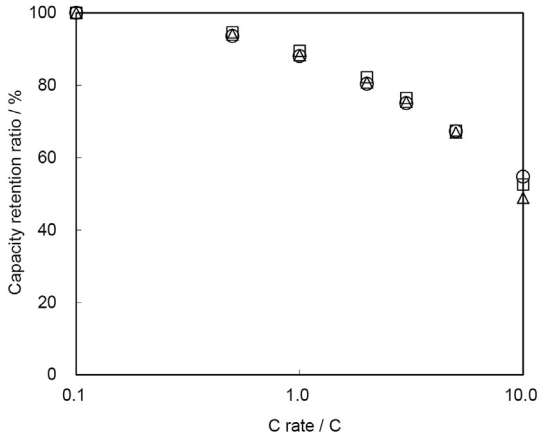

Fig. 8. Dependency of capacity retention ratios on the height (H) of LTO electrode line at various C rates, estimated using the cells with 3D-patterned electrodes of $H = 90$ μm (△), 70 μm (□), 50 μm (○). Both S and W values were fixed to 100 μm.

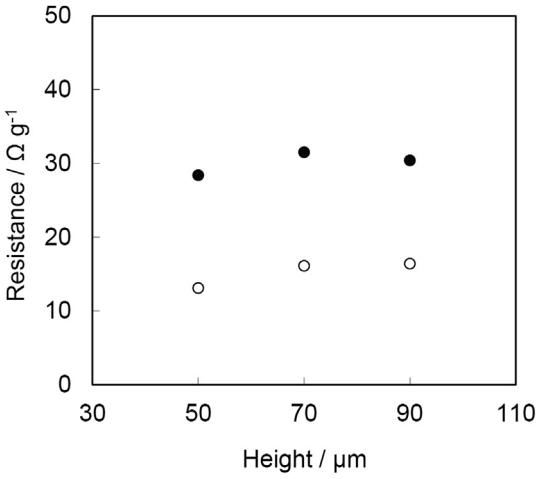

Fig. 10. Internal resistances of the cells with 3D-patterned electrodes of different H values, estimated at the charged (R_c: ○) and discharged (R_d: ●) states.

controlled to be 150 and 100 μm for $W = 70$ and 100 μm, respectively. The space (S) between two neighboring electrode lines was fixed to 110 μm. The charge and discharge test were carried out at the same conditions for Fig. 6. Fig. 11 shows the capacity retentions on C rate for the cells with the 3D-patterned LTO cathode with $W = 70$ and 100 μm. For the case of narrower electrode with $W = 70$ μm, higher capacity was obtained at over 10 C rates. The narrower 70 μm electrode cell kept the higher capacity. Therefore, the narrower width of electrode should be suited for enhancement of lithium-ion diffusion in the electrode.

As demonstrated above, the cell fabricated by using the 3D-patterned LTO cathode showed the rapid charge and discharge characteristics. Cyclic voltammetry test suggested that lithium-ion diffusion rate in the cell with 3D-patterned cathode is faster than that with conventional flat electrode, and rapid charge and discharge were realized. Their improvements are achieved by larger electrode surface area and shorter distance of lithium-ion diffusion length than those in conventional flat electrode. On the other hand, interfacial lithium-ion transfer resistance, namely R_{ct} estimated in AC impedance measurements was almost same regardless of the electrode structure. This result clearly demonstrates that R_{ct} depends on active material itself and not on the electrode structure. Therefore, the electrode performance can be optimized simply by the specifications of 3D-patterned electrode. The capacity per unit area is able to be improved without sacrificing the capacity retention ratio by increasing the height (H) of electrode line or reducing the space (S) between two neighboring electrode lines. On the contrary, the capacity retention ratio can be improved by fabricating the electrode line with narrower width (W). As expected in the previous report [11], it was confirmed that the higher aspect ratio (H value/W value) and the smaller space (S) are suited for improving the electrochemical performance of 3D-patterned electrode. Other active materials except LTO are also expected to be applicable for the 3D-patterned electrode by using the described method. The 3D-patterned electrode with high aspect ratio that stands on a current collector is a promising structure for high energy density and high rate performance of lithium-ion battery.

4. Conclusions

The effect of electrode specifications on the electrochemical performance of 3D-patterned electrode was thoroughly investigated. The height (H) of electrode hardly affects the capacity retention property of 3D-patterned electrode in a range of H value from 50 to 90 μm. Hence, the capacity per unit area can be increased simply as increasing the electrode height. The capacity can be also increased by reducing the space between two neighboring electrode lines (S) without sacrificing the rate performance of electrode. On the other hand, the 3D-patterned electrode with the narrower width of

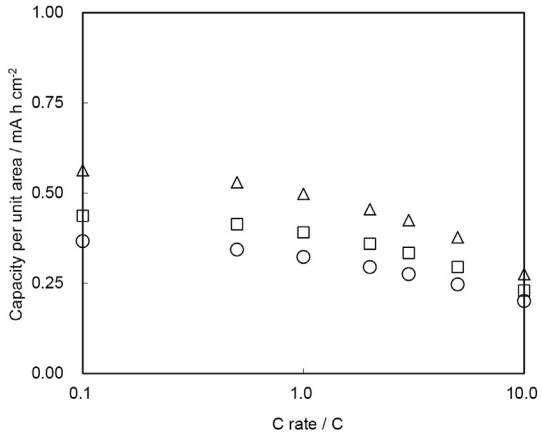

Fig. 9. Capacity dependency on C rate for the cells with 3D-patterned electrodes of different H values (Fig. 8): $H = 90$ μm (△), 70 μm (□), 50 μm (○).

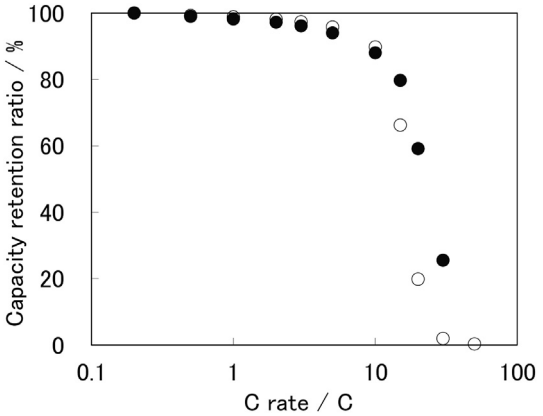

Fig. 11. Capacity retentions ratios as a function of C rate of the cells with different 3D-patterned electrodes (○: $W = 100$ μm, $H = 100$ μm, ●: $W = 150$ μm, $H = 70$ μm) but retaining the same capacity per unit area.

electrode line (W) showed the higher capacity retention ratio, suggesting that the rate performance of electrode strongly depends on the electrode width. This mechanism can be understood by considering the shorter diffusion length of lithium-ion in the electrode with narrower width. Consequently, the rate capability of electrode can be enhanced by achieving smaller W value, and the capacity can be increased as increasing H value or decreasing S value. In the 3D-patterned electrode, each electrode specification (W, H, S) is controllable individually. This feature is completely different from the case of conventional flat electrode and a great advantage of 3D-patterned electrode. Hence, rapid charge/discharge performance was realized in the cell with the 3D-patterned electrode. It was revealed by AC impedance measurements that charge-transfer resistance (R_{ct}) does not depend on the electrode structure. Thus, the superior rate capability of 3D-patterned electrode is essentially due to its specifications.

References

[1] K. Takeno, M. Ichimura, K. Takano, J. Yamaki, J. Power Sources 142 (2005) 298.
[2] N. Sato, J. Power Sources 99 (2001) 70.
[3] K. Kang, Y.S. Meng, J. Bréger, C.P. Grey, G. Ceder, Science 311 (2006) 977.
[4] N. Li, C.R. Martin, B. Scrosati, Electrochem. Solid State Lett. 3 (2000) 316.
[5] X. Ma, B. Kang, G. Ceder, J. Electrochem. Soc. 157 (2010) A925.
[6] R. Santhanam, B. Rambabu, J. Power Sources 195 (2010) 4313.
[7] Y. Tang, L. Yang, Z. Qiu, J. Huang, J. Mater. Chem. 19 (2009) 5980.
[8] Y. Wang, G. Cao, Adv. Mater. 20 (2008) 2251.
[9] C. Jiang, M. Wei, Z. Qi, T. Kudo, I. Honma, H. Zhou, J. Power Sources 166 (2007) 239.
[10] J.W. Long, B. Dunn, D.R. Rolison, H.S. White, Chem. Rev. 104 (2004) 4463.
[11] A. Izumi, M. Sanada, K. Furuichi, K. Teraki, T. Matsuda, K. Hiramatsu, H. Munakata, K. Kanamura, Electrochim. Acta 79 (2012) 218.
[12] K. Yoshima, H. Munakata, K. Kanamura, J. Power Sources 208 (2012) 404.
[13] H. Munakata, H. Sugiura, K. Kanamura, Funct. Mater. Lett. 2 (2009) 9.
[14] K. Dokko, J. Sugaya, H. Munakata, K. Kanamura, Chem. Lett. 34 (2005) 984.